Polymer xxx (2009) 1–8

Contents lists available at ScienceDirect

Polymer

journal homepage: www.elsevier.com/locate/polymer

Characterization of drawn monofilaments of liquid crystalline polymer/carbon nanoparticle composites correlated to nematic order

Estelle Kalfon-Cohen [a,*], Gad Marom [a], Ellen Wachtel [b], Alessandro Pegoretti [c]

[a] Casali Institute of Applied Chemistry, The Hebrew University of Jerusalem, 91904 Jerusalem, Israel
[b] Chemical Research Infrastructure Unit, The Weizmann Institute of Science, 76100 Rehovot, Israel
[c] Department of Materials Engineering and Industrial Technologies, University of Trento, Via Mesiano 77, 38100, Italy

ARTICLE INFO

Article history:
Received 11 November 2008
Received in revised form
1 February 2009
Accepted 4 February 2009
Available online xxx

Keywords:
Drawn monofilament
Carbon nanoparticles
Nematic order

ABSTRACT

In this study a nanocomposite monofilament composed of a nematic thermotropic liquid crystalline polymer (TLCP) mixed with 1.5 wt.% of carbon nanoparticles (CNP) was prepared by melt extrusion. The nanoparticles had either a fibrous (VGCF) or layered (GNP) geometry. The tensile strength and modulus of the fibers increased with the draw down ratio of the filament; a positive effect on the tensile modulus is displayed by fibrous CNP, achieving values higher than those of high property organic fibers utilized as reinforcement for composite materials. Thermotropic transitions were characterized by DSC and *in situ* synchrotron WAXD. In particular, it was shown that the breadth of the temperature span of the crystalline–nematic transition correlated inversely with the draw down ratio. At high draw down ratio, addition of CNP also increased the relative amount of oriented polymer chains and contributed to sharpening of the mesomorphic transition.

1. Introduction

Thermotropic liquid crystalline polymers (TLCPs) are probably the ideal candidates for preparing fibers by melt extrusion. In the melt, the degree of uniaxial orientation is typically very high and the extensional flow that is associated with the extrusion process orients the nematic regions in the flow direction [1]. Consequently, the resulting preferred orientation of the nematic phase of the TLCP imparts excellent tensile strength and modulus to the crystalline solid-state [2,3]. The nematic phase is characterized by positional short-range order of the mesogens; within a given domain, however, the molecules do possess quasi long-range orientational order of their long axes, which tend to lie parallel to a common axis labeled the director $\vec{n}$. A small orientating field is sufficient to align the directors, thereby effectively increasing the domain size. It is noted that a similar flow effect is observed in various polyolefins in which flow aligned stretched chains nucleate and crystallize in an oriented shish–kebab structure [4,5]. When an oriented solid TLCP is heated beyond its crystalline-nematic transition temperature (T_{CN}), the orientation is partially retained in textured microdomains, whose size, being related to the motion of the mesogens, is reduced as the temperature is raised. Above the melting transition temperature, the domain size of the mesophase is very small and the liquid displays the properties of an isotropic melt.

LCPs are intrinsically self-ordering at the molecular and nanoscale levels [5,6]. Under a shear or tensile stretching force the liquid crystalline domains respond by aligning the directors along the stretching direction [7]. The first challenge addressed in this study is to facilitate the inherent molecular orientation of the mesophase by applying an additional drawing force during the extrusion of the monofilaments and thereby to improve the mechanical properties as a function of the draw down ratio. Another state-of-the-art option for improving the mechanical properties of polymers is to reinforce them with small amounts of nanoparticles. Polymer nanocomposites have attracted considerable interest in polymer material research because of their potentially excellent mechanical properties [8]. In recent years various attempts have been made to develop high performance polymer nanocomposites, using nanoscale reinforcements of inherently high aspect ratio. Accordingly, a number of previous studies report on the utilization of organoclays [9,10] and carbon nanotubes [11] in TLCP, thereby causing significant improvement in the thermal and mechanical properties. Hence, the second challenge addressed in this study is the introduction into the TLCP filaments of nanoparticles which will serve as reinforcement and may also effect the molecular orientation. Previous studies by members of this research group have shown that by using two types of the same LCP fiber, namely Vectran M and Vectran HS, a new family of single polymer, self-reinforced

* Corresponding author. Tel.: +972 2 6586565; fax: +972 2 6586068.
E-mail address: estelle.kalfon@mail.huji.ac.il (E. Kalfon-Cohen).

0032-3861/$ – see front matter © 2009 Elsevier Ltd. All rights reserved.
doi:10.1016/j.polymer.2009.02.002

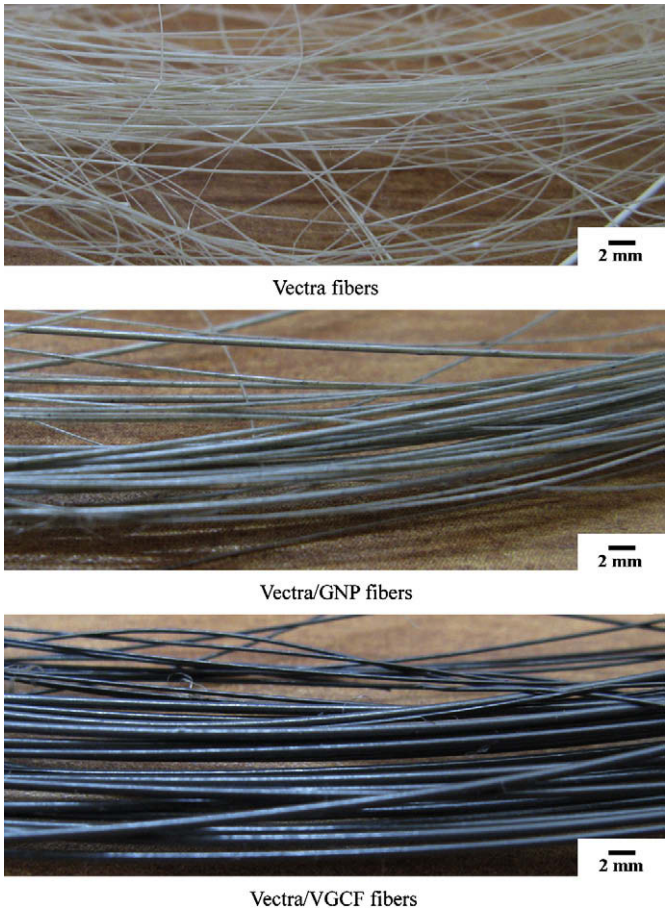

Fig. 1. Optical micrographs of the extruded fibers.

composites can be produced [12]. The apparent similarity between the extruded-drawn nanocomposite TLCP monofilaments of this study and the Vectran M filaments, suggests that the former can also be used as an improved matrix for such self-reinforced composites. The anticipated improvement is related to the reinforcing effect of some nanoparticles and their ability to induce enhanced oriented crystallinity under flow conditions.

The primary objective of this study is to analysis the morphology, considering the nematic mesophase, of drawn monofilaments of LCP/CNP nanocomposites and its consequences with respect to the mechanical properties. The orientation level resulting from the combination of DD and CNP addition is to be evaluated by *in situ* wide angle synchrotron X-ray diffraction, including the effect of the CNP geometry and its interaction with nematic domains.

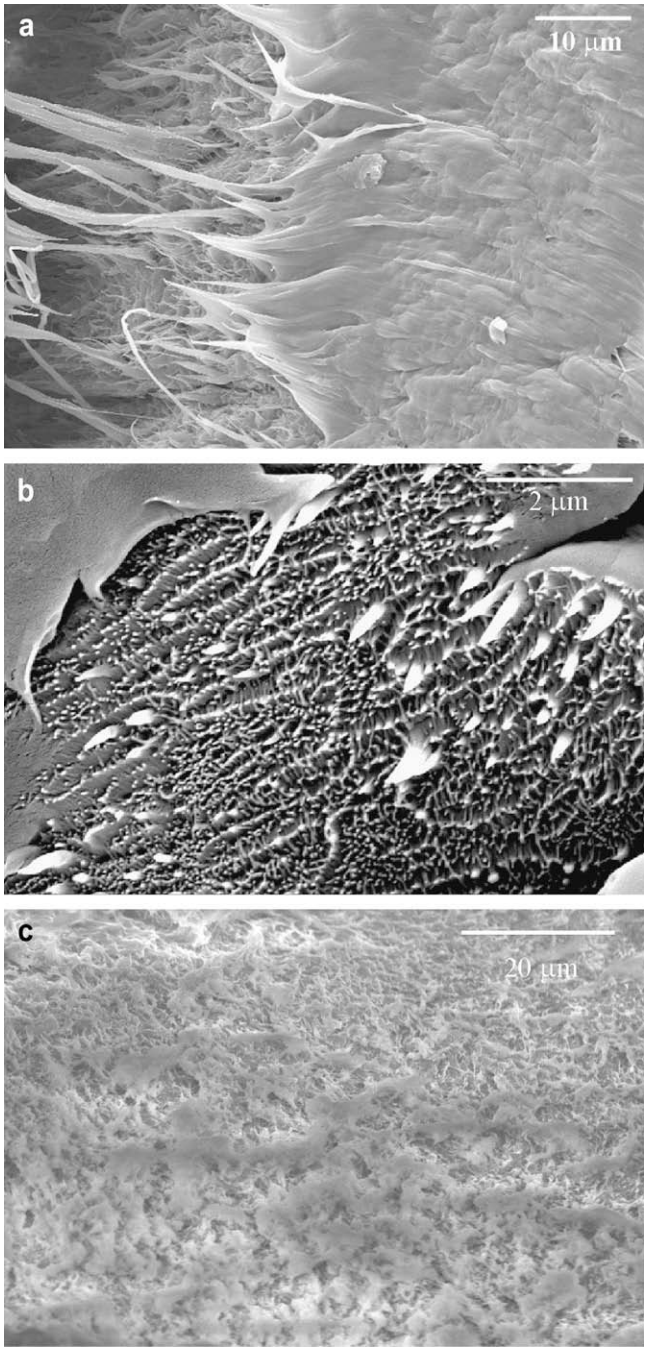

Fig. 2. SEM micrographs of vectra (a), vectra/GNP (b) and vectra/VGCF (c) at DD = 5. The monofilaments were sliced after freezing.

2. Experimental

2.1. Materials

The TLCP used in this study is Vectra A950, Ticona. This is an aromatic copolyester composed of 1,4-hydroxybenzoic acid (HBA) and 2,6-hydroxynaphtanoic acid (HNA) in a molar ratio of 73/27 respectively [13]. The random copolymerization of HNA and HBA disrupts the registry between the adjacent chains thereby reducing the crystal to nematic transition temperature. The HNA monomer has a larger transverse size than that of the HBA monomer, a fact which results in an increase in the inter-chain distance, and a dramatic lowering of the melting temperature. Vectra A950 has a glass transition at 110 °C and a nominal crystal to nematic transition at 276 °C. Vapor grown carbon nanofibers VGCF-H (graphitized up to 2800 °C) were supplied by Showa Denko KK, Japan. The average diameter and length of the VGCF are 150 nm and 10–20 μm respectively; their density is 2 g/cm^3.

Graphite nano-platelets (GNP) were prepared according to the method described in our previous studies [14] and provided by J.K. Kim of HKUST-Hong Kong. A graphite intercalation compound (GIC) that contained 2.8 wt.% of sulfur as intercalant (supplied by Asbury Graphite Mills, USA) was put into an oven that was maintained at 1050 °C and taken out after 30 s to produce expanded graphite. Upon rapid heating the GIC expanded explosively several hundred times along the thickness direction as a result of the evaporation of

Please cite this article in press as: Kalfon-Cohen E et al., Polymer (2009), doi:10.1016/j.polymer.2009.02.002

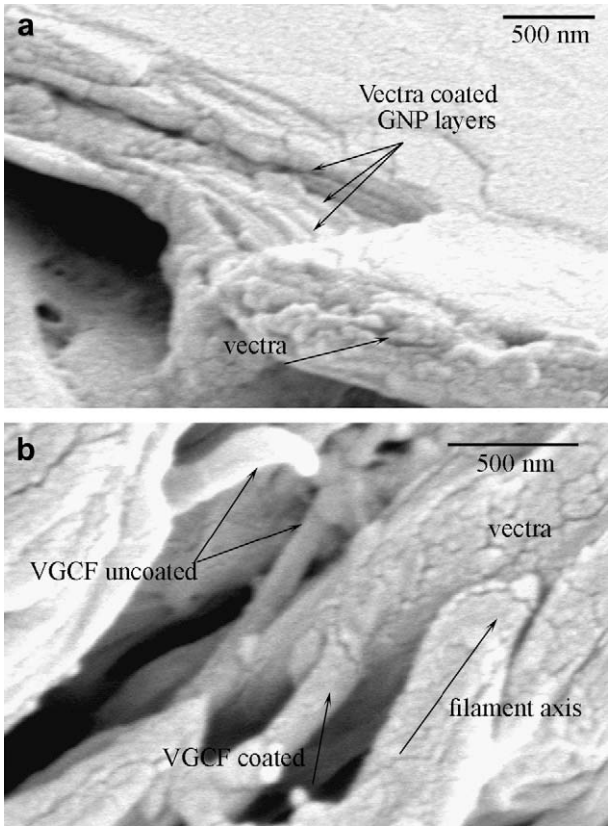

Fig. 3. Higher magnification SEM micrographs of GNP layers or VGCF inclusions in vectra/GNP (a) and vectra/VGCF (b) monofilaments at DD = 5.

the intercalant and the thermal shock. The expanded graphite was immersed in acetone and ultrasonicated at 70 W and 42 kHz for 8 h to obtain exfoliated GNPs. The average thickness and diameter of the GNPs were estimated to be 4.5 nm and 46 μm, respectively [14].

2.2. Extrusion of filaments

Melt mixing of Vectra A950 pellets filled with 1.5 wt.% of VGCF or 1.5 wt.% of GNP, was carried out in a twin-screw micro-compounder (DSM, Netherlands). Mixing was performed at 293 °C for a period of 10 min, according to the procedure published elsewhere [15]. This was followed by extrusion through a 900 μm die and drawing of fiber-like filaments with diameters decreasing from 900 μm to 30 μm (with corresponding draw down ratios DD = 1 to DD = 900). Optical micrographs of as-extruded monofilaments are presented in Fig. 1.

2.3. Electron microscopy

The morphology and the distribution of the nanoparticles across the cross-section of extruded filaments were examined by high-resolution scanning electron microscopy HRSEM (Sirion 200, FEI). The fibers were first immersed in liquid nitrogen and then sectioned with a sharp knife.

2.4. Thermal analysis

Differential scanning calorimetry DSC (Mettler 822e Toledo, Switzerland) thermograms were measured in the temperature range 20–400 °C at a heating rate of 10 °C/min under a nitrogen flux of 50 ml/min. The weight of each sample was about 10–15 mg.

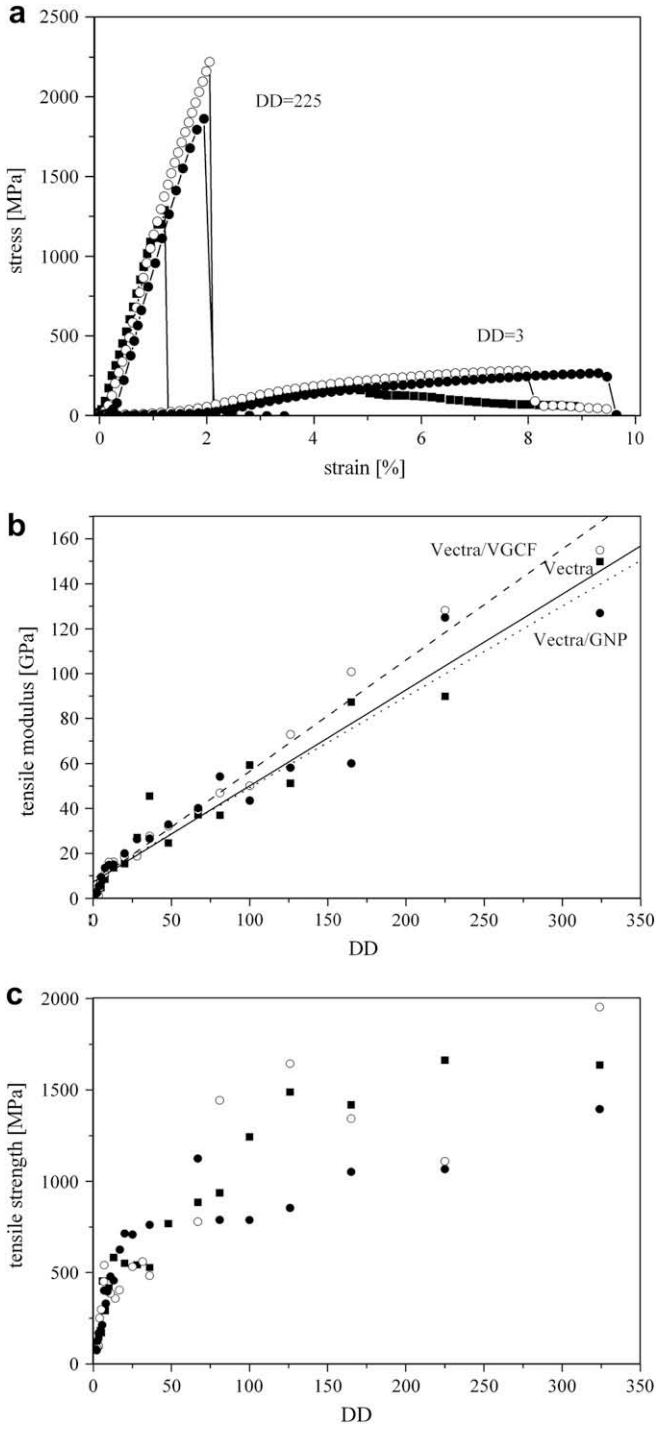

Fig. 4. Stress–strain curve (a), tensile modulus (b) and tensile strength (c) of (■) vectra (●) vectra/GNP and (○) vectra/VGCF monofilaments as a function of DD. The lines in Fig. 4b express the linear regression of (—) vectra, (- - -) vectra/VGCF and (. . .) vectra/GNP monofilaments.

2.5. In situ WAXD measurement

Synchrotron microbeam WAXD measurements were performed at the ESRF in Grenoble (France) on the Materials Science Beamline (ID-11). The X-ray microbeam was monochromated at a wavelength of $\lambda = 0.4875$ Å and collimated to dimension 2 μm (vertical) by 4 μm (horizontal). The exposure time for each sample varied from 20 to 60 s. Samples were inserted into 0.5 or 1 mm diameter Li–glass capillaries and mounted inside a hot stage (Linkam Scientific

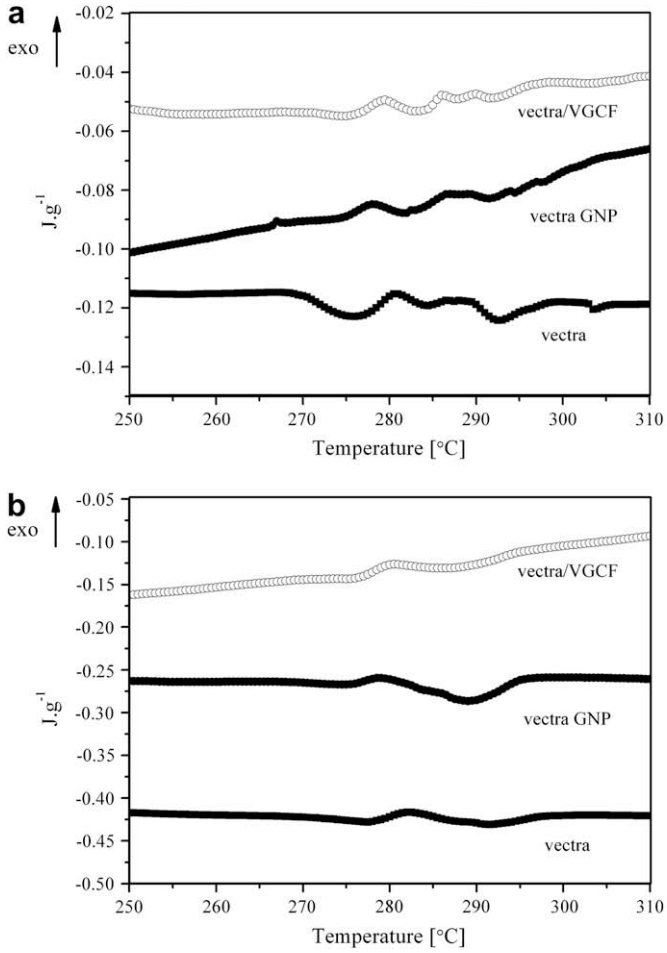

Fig. 5. DSC thermograms of as-extruded filaments at DD = 165 (a) and DD = 5 (b). The scan rate was 10 °C/min.

Instruments, THMS600, Waterfield, UK). The distance between the sample and the detector was set at approximately 143 mm. Each sample was scanned during heating at 10 °C/min from 25 to 400 °C. Data were taken at 5 or 10 °C intervals. The one-dimensional diffraction profiles were calculated from the two-dimensional X-ray diffraction patterns using the image analysis programs Fit2D (ESRF, Dr Hammersley) and Polar (SUNY, Stony Brook, NY). Azimuthal scans performed in Polar permitted the separation of the oriented and non-oriented contributions to the total intensity of the diffraction pattern. The isotropic fraction $A_{iso}(s)$ can be extracted by using the "*Halo*" method described below. Starting from the center of the scattering pattern, a series of azimuthal scans can be obtained as a function of s ($[s = 2\sin(\theta/2)/\lambda]$ is the scattering vector and θ is the scattering angle). All the minimum intensity values of the sequential azimuthal scans thus represent the envelope of the isotropic contribution.

The anisotropic fraction $A_{an}(s, \varphi)$ then can be calculated from the following equation:

$$A_{an}(s,\varphi) = A(s,\varphi) - A_{iso}(s) \quad (1)$$

where $A(s, \varphi)$ is the total scattering and φ is the azimuthal angle. The method is fully detailed in Ref. [16].

2.6. Mechanical testing

Tensile testing was performed on an universal testing machine (Instron, Model 4502) at a gage length of 20 mm and loading rate of 10 mm/min. At least 10 specimens were tested for each composition and draw down ratio. For three high draw down ratios, the scatter in the tensile strength data was analyzed using the Weibull distribution on samples consisting of 15 specimens [17]:

$$P(\sigma) = 1 - \exp\{-(\sigma/\sigma_0)^m\} \quad (2)$$

where $P(\sigma)$ is the cumulative failure probability of a fiber at stress σ, while σ_0 and m represent the scale and the shape Weibull parameters, respectively.

3. Results and discussion

3.1. Microscopic characterization and mechanical properties

Fig. 2 presents cross-sections of as-extruded monofilaments which were sliced after freezing. It clearly emerges that both types of CNP significantly reduce the fibrillation and plastic deformation typically observed in the pristine polymer. The fracture surfaces of the CNP-filled monofilaments exhibit the typical features of a semi-brittle fracture with only limited plastic deformation. Fig. 3 presents high magnification fracture micrographs of the as-extruded monofilaments filled with VGCF or GNP. Two interesting features can be observed, namely, that the individual VGCF particles are oriented along the filament axis, while layered (un-exfoliated) GNP are embedded in the polymer with no specific orientation.

Fig. 4a shows the stress–strain curves under tensile testing of vectra filaments, without and with CNP, for two extreme DD. The same clear trend observed for the three monofilaments is that as DD is increased the fiber breaking strain is reduced, while the stress level values are increased, showing a transition from ductile to brittle behavior. Consequently, for all the samples, increasing the DD improves both the tensile modulus and the tensile strength. At low DD, i.e. from DD = 1 to 40, the tensile modulus (Fig. 4b) increases rapidly from 2 to 30 GPa, for all three filament types. At higher DD, i.e. up to DD = 325, the measured tensile modulus increases more gradually up to values in the range 120–140 GPa. The lines in Fig. 4b express the linear regression results for the three sets along the whole draw down ratio range. The data for vectra/VGCF filaments display the best fit (with $R^2 = 0.99$ and standard deviation of about 6 GPa) and an average tensile modulus higher than 140 GPa is reached at DD = 325. The data for vectra and vectra/GNP filaments display large scatter–linear regression ($R^2 = 0.97$; standard deviation of 8 GPa and $R^2 = 0.96$; standard deviation of 9 GPa respectively). The geometry of the CNP therefore plays a role in determining the mechanical response of LCP filaments. Due to their high aspect ratio, VGCF can align in the melt under flow, thus providing excellent tensile properties compared to nanoplatelets. It is worthwhile to note that the modulus values obtained here are much higher than those of commercially available vectran untreated (84 GPa) and thermally treated (89 GPa) fibers [12]. Moreover, the modulus value of vectra/VGCF at DD = 225 is 128 GPa, which is comparable or even higher than the moduli of high property organic fibers, such as aramid (~120 GPa) and polyethylene (~124 GPa), utilized as reinforcement for composite materials.

The tensile strength results are shown in Fig. 4c. Up to DD ~ 30, the tensile strength approximately linearly increases for the three types of filaments, reaching ~500 MPa. Beyond DD = 30, the tensile strength of vectra/GNP filaments is an approximately linear function of DD and is consistently lower than that of vectra or vectra/VGCF filaments, reaching ~1.3 GPa at DD = 325. The data for vectra and vectra/VGCF are subjected to a large scatter. Weibull distribution analysis of 16 specimens of unfilled vectra fibers with draw down ratio of 225, furnished a scale parameter $\sigma_0 = 1726$ MPa

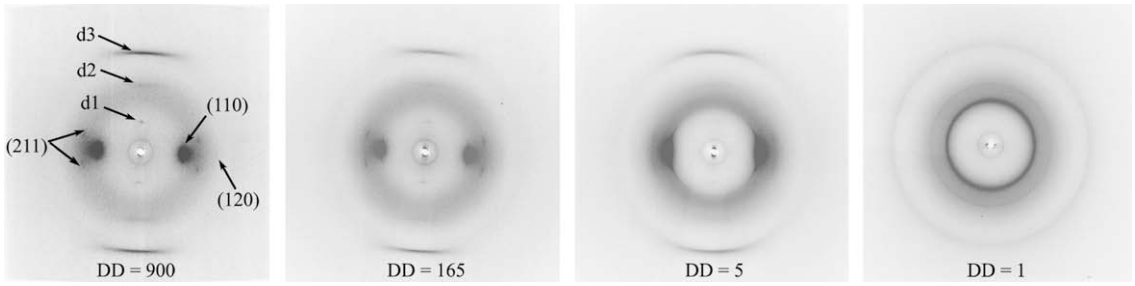

Fig. 6. Room temperature 2D WAXD patterns of vectra filaments for four DD. The most prominent diffraction peaks are identified for DD = 900. The ring closest to the beam stop is instrumental in origin.

and a shape parameter $m = 2.26$. These parameters, referred to a gage length of 20 mm, can be compared with those of commercially available untreated vectran fibers (vectran M) of the same gage length, i.e. $\sigma_0 = 1309$ MPa and $m = 8.28$, respectively [12]. It can therefore be concluded that drawing and the resulting orientation generate significantly improved tensile strength, but with a variability much larger than that of similar commercial fibers. The parameters of the Weibull distribution function for filled monofilaments with draw down ratio 225, resulted to be $\sigma_0 = 1157$ MPa and $m = 7.05$ and $\sigma_0 = 1553$ MPa and $m = 6.01$ for vectra/GNP and vectra/VGCF, respectively. These values approximately fit the average results shown in Fig. 4c. As the DD is increased, the required drawing force on the monofilament must be significantly higher and consequently defects are created within the fiber. The combination of nanoparticles and high draw down ratio seems to amplify such defect formation being responsible for the early failure in the composite monofilament as compared to the pristine fiber. It is also possible that the effect of the CNP on the mechanical properties and probably also on the degree of scatter in the data may be a consequence of non-uniform dispersion of CNP aggregates. This lack of uniform dispersion is associated with the relatively simple melt mixing procedure employed. Although the aggregated CNP were effective nucleants, they did not posses a suitable aspect ratio for reinforcement.

3.2. Thermotropic transitions and filament structure

The drawn LCP fibers were studied by differential scanning calorimetry as well as by synchrotron X-ray diffraction. Fig. 5 presents the thermograms obtained during heating of the extruded polymer filaments at two different draw down ratios. It is noted that the transition enthalpies in the thermograms are very low. Based on our previous study [18] and literature data [19] we may identify endotherms as follows. Two endotherms are observed for the undrawn filament at 277 ± 1 °C and at 290 ± 2 °C while several low enthalpy endotherms are observed in the drawn filament. However, it can be noted that for the latter, prominent endotherms also occur at 280 ± 2 °C, and at 291 ± 2 °C. A scan at 30 °C/min for the DD = 165 filaments (not presented here) show only two endotherms: at 275 °C and 293 ± 2 °C. The multiple endotherms may have been induced by the different thermal histories between the skin and the core of the polymeric filament. It can also be observed that addition of CNP has only a minor effect on the temperature and on the enthalpy of the peaks. It is well known that upon cooling, random copolymers such as vectra display a rapid crystallization process to a pseudo-hexagonal (PH) phase and a slow crystallization process to an orthorhombic phase [19]. As will be shown below, a mixture of the two phases is observed in the extruded filament. In this case, the lower temperature endotherm can be assigned to a change from the solid crystalline state with mixed orthorhombic/PH structure to less ordered crystals in the PH phase. The second endotherm is assigned to the transition from the PH crystals to the nematic liquid crystal phase [19,20].

Structural analysis of vectra filaments using WAXD reveals that the molecular organization of the drawn fibers at room temperature is typical of a semi-crystalline polymer with a low degree of crystallinity, containing a mixture of oriented and un-oriented chains. X-ray diffraction patterns of vectra filaments at low and high draw down ratios are presented in Fig. 6. An enhanced orientation of the crystals is observed as the draw down ratio is

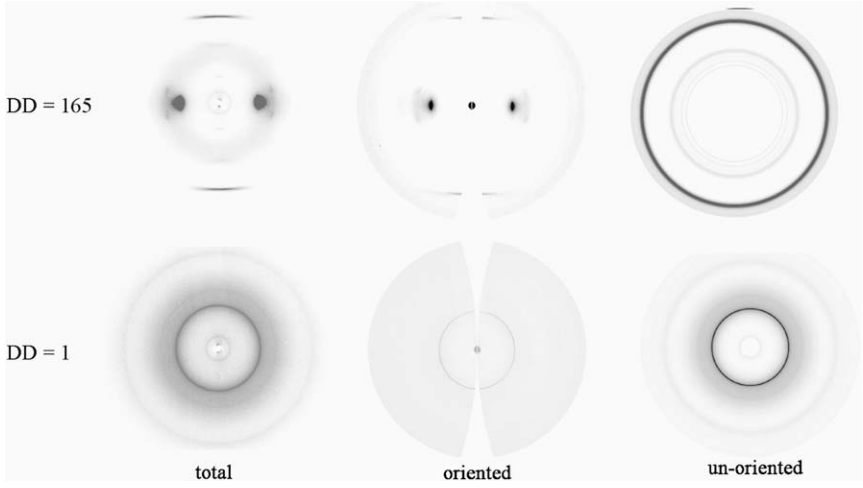

Fig. 7. Typical room temperature diffraction patterns of vectra/GNP filaments separated into oriented and un-oriented fractions [16].

Please cite this article in press as: Kalfon-Cohen E et al., Polymer (2009), doi:10.1016/j.polymer.2009.02.002

Table 1
Relative diffraction intensity of oriented and isotropic fractions.

DD	Vectra		Vectra/GNP		Vectra/VGCF	
	Oriented [%]	Isotropic [%]	Oriented [%]	Isotropic [%]	Oriented [%]	Isotropic [%]
1	20	80	19	81	27	73
5	37	63	39	61	40	60
81	40	60	46	54	49	51
165	49	51	44	56	59	41
900	59	41	52	48	92	8

Table 2
ψ-FWHM (°) calculated from the azimuthal scan of the (110) reflection after subtraction of the isotropic fraction.

DD	Vectra	Vectra/GNP	Vectra/VGCF
1	70	90	90
5	26	12	11
81	9	11	10
165	10	11	8
900	10	7	6

increased. The crystalline structure of the extruded filaments of vectra can be more easily understood by comparing these data with those previously obtained on Vectran® M and Vectran® HS fibers [20], In filaments with high draw down ratio, the so-called pseudo-hexagonal (PH) crystalline structure is revealed by the presence of two intense diffraction maxima, one on the equator, assigned to the (110) planes and the second on the first layer line, due to the (211) planes [21]. Three meridional reflections are also observed at $2\theta \approx 4.09^\circ$ (strong), $2\theta \approx 9.39^\circ$ (weak) and $2\theta \approx 13.75^\circ$ (weak) labeled here as d_1, d_2, and d_3 respectively. No crystallographic indexing of these peaks is possible due to the random axial arrangement of the copolymer. As the draw down ratio is decreased, only d_3 is retained while d_1 and d_2 are no longer observed. This is likely due to azimuthal smearing of the reflection intensities. In general, vectra, which is a random copolymer of HBA and HNA, shows a splitting of the (110) and the (200) reflections indicating an orthorhombic structure. In our case no splitting was discernable, probably because of the very strong amorphous ring centered near the (110) reflection. However, when the draw down ratio was increased to 165, an additional reflection was observed at $2\theta \approx 11^\circ$ and assigned to the (120) planes. The observation of the weak (120) reflection, only observed in the orthorhombic phase [21], is likely due to the improved orientation and resulting azimuthal concentration of the intensity. The appearance of the (120) peak implies that at least a fraction of the polymer chains is arranged in an orthorhombic structure even if the (200) reflection is not observed in the pattern.

The total diffracted intensity in the 2D WAXD patterns can be deconvoluted into contributions from the oriented and un-oriented chains (Fig. 7), as described in Section 2. The relative contributions of oriented and isotropic chains to the intensity of the room temperature diffraction patterns of vectra and vectra/CNP filaments with various draw down ratios are presented in Table 1. Two main conclusions can be drawn. Addition of VGCF to the undrawn filament seems to moderately enhance the oriented fraction (by 35%) while addition of GNP slightly reduces it. The combination of addition of VGCF with tensile stretching (DD = 900) raises the oriented fraction by a factor of 4–5. After passing a stress threshold (DD ≈ 200), the intrinsic anisotropy of nanofibers causes them to align and leads to this improvement. The aspect ratio of the CNP has an influence on the molecular orientation of the polymer during extrusion. Whereas a fibrous CNP such as VGCF can align with the intrinsic orientation of the melt, a layered CNP like GNP disturbs the alignment and reduces the orientation. If additional drawing force is applied to the nematic phase, the fibrous particles will align parallel to the flow direction and will enhance the molecular

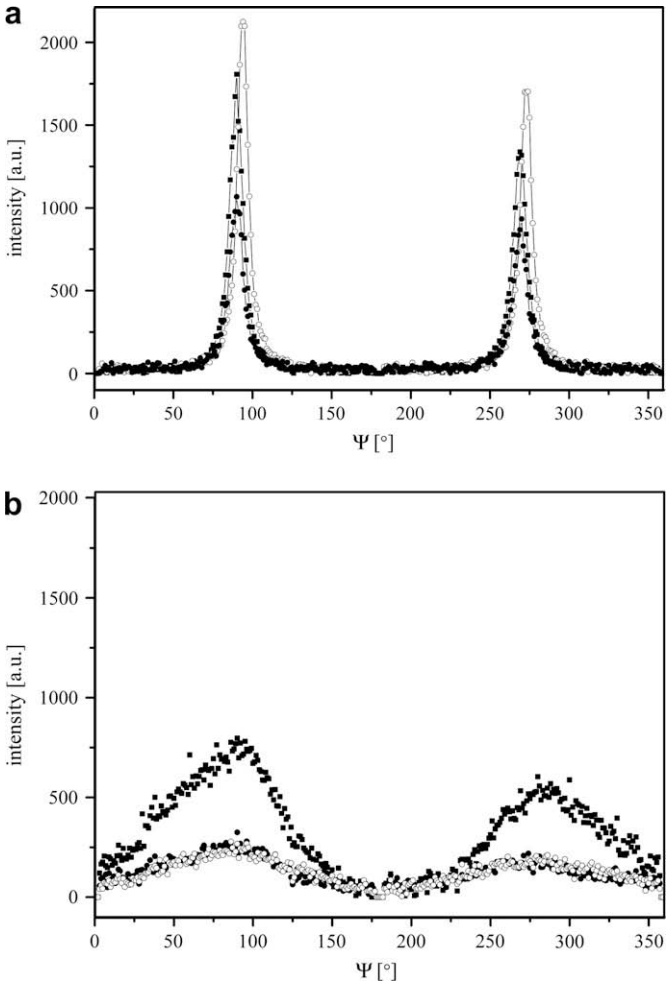

Fig. 8. Azimuthal (Ψ) scans of the (110) reflection measured at room temperature for (■) vectra (●) vectra/GNP (○) vectra/VGCF filaments at DD = 165 (a) and DD = 1 (b).

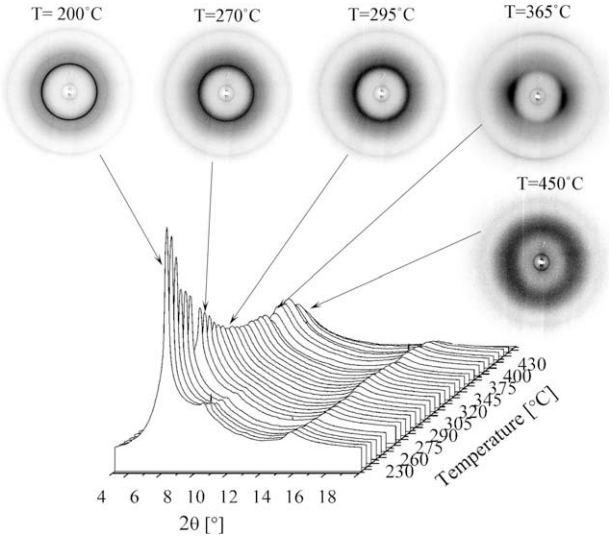

Fig. 9. 2D WAXD patterns and the corresponding circular averages obtained during *in situ* heating of a vectra filament (DD = 1).

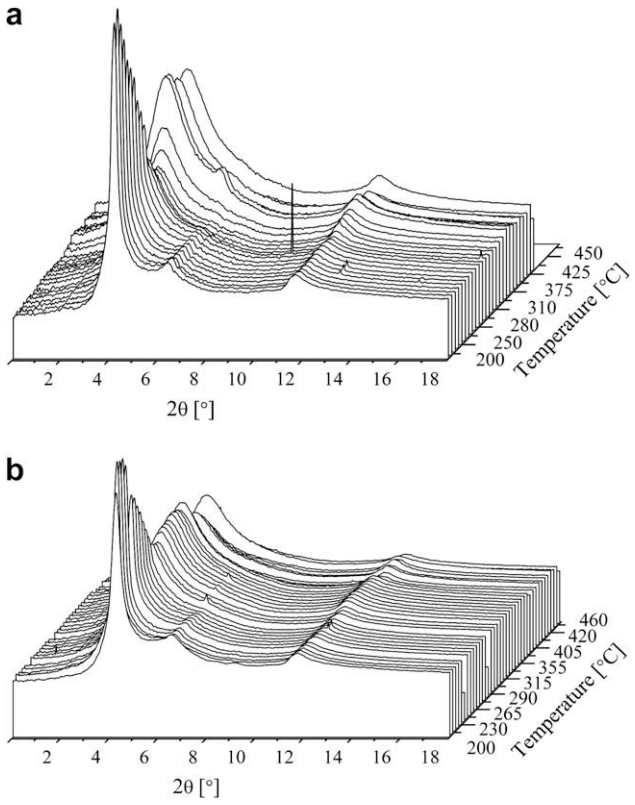

Fig. 10. Circular averages of 2D WAXD patterns during *in situ* heating of vectra/VGCF (a), vectra/GNP (b), both with DD = 1.

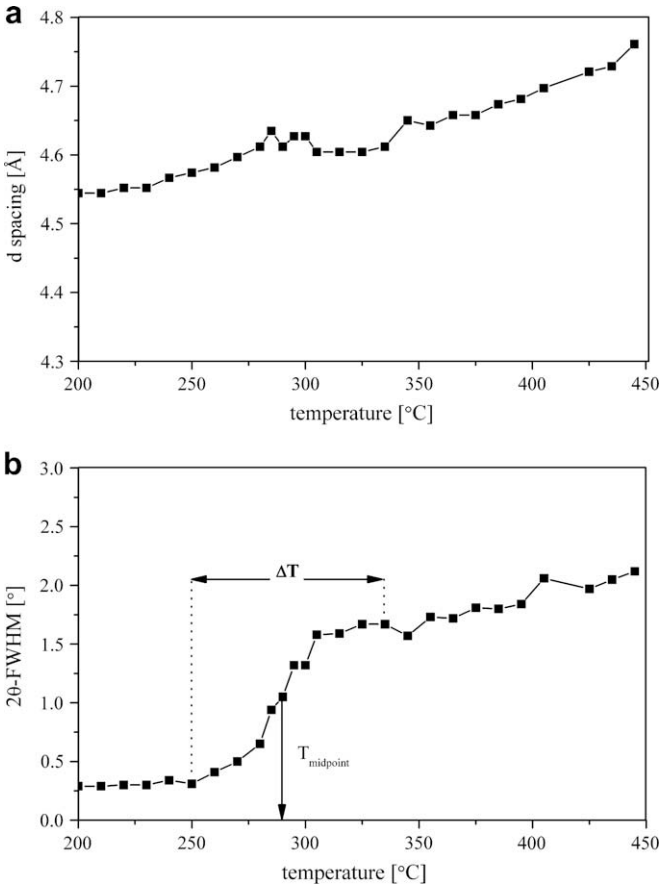

Fig. 11. Changes in d (a) and 2θ-FWHM (b) of the (110) reflection during heating of a vectra/GNP filament, DD = 1.

orientation [22]. However, in previous studies on vectra/nanofiber composites [23,24] it was shown that addition of nanofibers reduces the anisotropy of the material, because of the anchoring effect of the CNP, which disturbs the nematic order. Nematic liquid crystals in contact with solid substrates or filler often adopt a preferred direction of alignment, referred to as anchoring. In our case, when the VGCF is combined with a high draw down ratio, the fibrous filler has a positive effect on the nematic order. If no drawing is applied, the CNP actually disturb the nematic order and reduce the anisotropy. On the other hand, a high draw down ratio results in a marked alignment of the filler particles which, due to their anchoring effect, improves the orientation of the mesogens along the fiber axis. As it will be shown below, a high anisotropic fraction may have a major impact on the nature of the thermotropic transition.

The effect of the draw down ratio on polymer orientation at room temperature can be evaluated quantitatively by profile fitting the azimuthal scan of the (110) reflection. Scans for each of the three filaments are superposed in Fig. 8a (DD = 165) and Fig. 8b (DD = 1). The azimuthal *full-width half-maximum* (Ψ-FWHM) of the (110) diffraction peak decreases with increasing draw down ratio by approximately one order of magnitude (see Table 2). The major effect is played by the DD; only minor differences are observed after the addition of CNP fillers, both at low or high draw down ratio.

The thermal transitions in the polymer are observed by *in situ* WAXD. During heating of the unfilled vectra with DD = 1, the evolution of the 2D WAXD patterns and the circular averages reveal four different states as shown in Fig. 9. Up to 200 °C, three well-defined diffraction peaks are observed. As the temperature is raised, the intensity of the peaks is reduced as seen at 270 °C and only the (110) and d_3 reflections are retained. Above the crystalline–nematic transition, the diffraction pattern is diffuse and weakly anisotropic, as observed at 295 °C. The equatorial reflection represents the average correlation distance between two adjacent mesogens and is observed at lower 2θ as the temperature is raised. The increased vibrational energy during heating to more than 450 °C increases the motion of the mesogens. The anisotropy of the melt is retained because of the intrinsic geometry of the copolymer skeleton, but molecular motion is already significant, thereby increasing the distance between two mesogens. Whereas the crystalline molecules in the solid-state lose their long-range order, the amorphous chains in the solid-state present a short-range order specific of the nematic state. As a consequence, the intensity of the liquid crystalline reflection is increased due to the contribution of both phases as seen at 365 °C. At 450 °C the fiber is almost completely amorphous and isotropic.

The circularly averaged 2D WAXD patterns acquired during heating of the CNP-filled filaments are presented in Fig. 10. We can identify similar behavior as that observed for the unfilled filaments. The same three reflections as those observed in the pristine vectra filament are seen in low temperature CNP-filled filaments. The

Table 3
Width of the crystal to nematic transition (ΔT (°C)) based on the 2θ-FWHM (°) of the 110 reflection in the circularly averaged profiles.

DD	Vectra	Vectra/GNP	Vectra/VGCF
1	65	65	50
5	45	60	50
81	40	45	45
165	45	30	30
900	45	30	20

(002) diffraction peak of carbon expected at $2\theta \approx 8.37^{\circ}$ is apparently overlapped by the (211) reflection of vectra and, consequently, it is not detected. At approximately 285 °C, when the three dimensional order of the polymer is lost, then the carbon (002) reflection can be observed. The disappearance of the crystalline structure of the polymer is followed by an increase in the intensity of the main equatorial reflection characteristic of the nematic state.

To correlate the thermotropic transitions observed in DSC and those observed by *in situ* WAXD, the d spacing (d) of the main equatorial reflection (110) can be plotted as a function of temperature (Fig. 11a). The equatorial reflection represents the average correlation distance between two adjacent mesogens and is observed at progressively lower 2θ as the temperature is raised. The increased vibrational energy during heating to more than 450 °C increases the motion of the mesogens. In the nematic phase the diffraction pattern is anisotropic but diffuse.

It is also useful to plot the radial 2θ-FWHM of this reflection during heating. The 2θ-FWHM of the equatorial diffraction is inversely proportional to the correlation length. In Fig. 11b we see that the FWHM may be fitted to a sigmoidal curve for which the temperature at the midpoint (T_{mid}) and the range of the transition can be determined by differentiation. These two parameters can then be evaluated as a function of the draw down ratio and the type of filament. The values of T_{mid} determined for all samples are in the range of 280–290 °C and are comparable to the second transition observed in the DSC thermograms. No systematic trend was observed as the draw down ratio is increased or CNP added. On the other hand, the width of the temperature range ΔT required for the material to organize in the nematic phase is highly sensitive to both as shown in Table 3 For the undrawn filaments the polymer seems to complete the transition to the nematic state at higher temperature than for the drawn ones, or in other words the transition to the nematic phase is significantly broader. The amorphous fraction in the oriented phase is increased and then aligns along the draw direction. It can be then understood that as the draw down ratio is increased ΔT is reduced and all the mesogens (previously in the crystalline and in the amorphous fraction) align within the mesophase. The addition of VGCF to the vectra filament further reduces ΔT by about 40%. This is probably due to the anchoring effect of the oriented nanofibers on the mesogen arrangement generating higher alignment in the solid-state as shown in Table 1 in which a fraction of 90% of the molecules is oriented at DD = 900.

4. Conclusions

Vectra fibers and fibrous nanocomposites containing 1.5 wt.% of GNP or VGCF were successfully prepared by a melt mixing and extrusion process. The mechanical behavior under tensile configuration is markedly improved with increasing draw down ratio, with a positive effect on the tensile modulus displayed by fibrous CNP, achieving values higher than those of high property organic fibers utilized as reinforcement for composite materials. In order to investigate the effect of draw down ratio and CNP on the structure of the fibers, a combination of *in situ* WAXD and DSC techniques was employed. By calculating the fraction of oriented and isotropic phases within the monofilaments, we have been able to show that, as expected, the relative amount of oriented phase increases with the draw down ratio for both unfilled and filled fibers. At high draw down ratios, among the three types of filaments, vectra/VCGF fibers contain the largest fraction of oriented chains. In parallel, these fibers display the sharpest thermotropic transition from the crystalline to the nematic phase.

For the three types of monofilaments a mixture of orthorhombic and pseudo-hexagonal structures was found. In DSC the two principal endotherms were assigned to the conversion of the orthorhombic fraction to the PH phase while the second transition was assigned to the conversion of the PH crystals to a nematic phase (T_{CN}). The change in the width of the (110) X-ray diffraction peak as a function of temperature permits determination of the midpoint of the crystalline–nematic transition and also the temperature breadth of the transition. We found that both the draw down ratio and the resulting amount of oriented phase have a major influence on the width of the crystalline–nematic transition. Favorable geometry of the CNP seems to enhance the polymer orientation only above a threshold draw down ratio. Fibrous CNP combined with high DD can act as a strong anchoring agent leading to an improvement in orientation and a reduction in the transition width.

References

[1] Ide Y, Ophir Z. Polymer Engineering and Science 1983;23:261–5.
[2] Chung TS. Journal of Polymer Science Part C 1986;24(7):299–303.
[3] Avila-Orta CA, Burger C, Somani R, Yang L, Marom G, Medellin-Rodriguez FJ, et al. Polymer 2005;46(20):8859–71.
[4] Dikovsky D, Marom G, Avila-Orta CA, Somani RH, Hsiao BS. Polymer 2005;46(9):3096–104.
[5] Donald AM, Windle AH. Liquid crystalline polymers. In: Cahn RW, Davis EA, Ward IM, editors. Cambridge solid state science series. Cambridge: Cambridge University Press; 1992. p. 235–60.
[6] Sawyer LC, Jaffe M. Journal of Materials Science 1986;21(6):1897–913.
[7] Zhao Y, Roche P, Yuan G. Macromolecules 1996;29(13). 4619–25.
[8] Romo-Uribe A. Rheologica Acta 2007;46(9):1139–52.
[9] Hussain F, Hojjati M, Okamoto M, Gorga RE. Journal of Composite Materials 2006;40(17):1511–75.
[10] Luo JJ, Daniel IM. Composites Science and Technology 2003;11(63):1607–16.
[11] Chang JH, Seo BS, Hwang DH. Polymer 2003;43(10):2969–74.
[12] Pegoretti A, Zanolli A, Migliaresi C. Composites Science and Technology 2006;66(13):1970–9.
[13] Yoon HN, Charbonneau LF, Clundann GW. Advanced Materials 1992;4(3):206–14.
[14] Green M, Marom G, Li J, Kim JK. Macromolecular Rapid Communications 2008;29(14):1254–8.
[15] Vaisman L, Larin B, Davidi I, Wachtel E, Marom G, Wagner HD. Composites Part A 2007;38(5):1354–62.
[16] Ran S, Zong X, Fang D, Hsiao BS, Chu B, Cunniff PM, et al. Journal of Materials Science 2001;36(13):3071–7.
[17] Weibull W. Journal of Applied Mechanics 1957;18:293–7.
[18] Kalfon Cohen E, Marom G, Weinberg A, Wachtel E, Migliaresi C, Pegoretti A. Polymer for Advanced Technologies 2007;18(9):771–9.
[19] Habenschuss A, Varma-Nair M, Kwon YK, Ma J, Wunderlich B. Polymer 2006;47(7):2369–80.
[20] Langelaan HC, de Boert Posthuma. Polymer 1996;37(25):5667–80.
[21] Wilson DJ, Vonk CG, Windle AH. Polymer 1993;34(2):227–37.
[22] Yudin VE, Svetlichnyi VM, Shumakov AN, Schechter R, Harel H, Marom G. Composites A 2008;39(1):85–90.
[23] Lee S, Kim MS, Naskar AK, Ogale AA. Polymer 2005;46(8):2663–7.
[24] Rohatgi A, Thomas JP, Baucom JN, Pogue WR, Cerully LB, Ebenstein DM, et al. Scripta Materialia 2008;58(1):25–8.